



Contents lists available at ScienceDirect

Ultramicroscopy

journal homepage: www.elsevier.com/locate/ultramic

High resolution imaging of surface patterns of single bacterial cells

Dominik Greif¹, Daniel Wesner¹, Jan Regtmeier*, Dario Anselmetti

Experimental Biophysics and Applied Nanoscience, Bielefeld University, Universitätsstraße 25, 33615 Bielefeld, Germany

ARTICLE INFO

Article history:

Received 13 October 2009

Received in revised form

26 April 2010

Accepted 1 June 2010

Keywords:

AFM

SEM

Artefact

Cell surface

Life cell imaging

Sample preparation

ABSTRACT

We systematically studied the origin of surface patterns observed on single *Sinorhizobium meliloti* bacterial cells by comparing the complementary techniques atomic force microscopy (AFM) and scanning electron microscopy (SEM). Conditions ranged from living bacteria in liquid to fixed bacteria in high vacuum. Stepwise, we applied different sample modifications (fixation, drying, metal coating, etc.) and characterized the observed surface patterns. A detailed analysis revealed that the surface structure with wrinkled protrusions in SEM images were not generated *de novo* but most likely evolved from similar and naturally present structures on the surface of living bacteria. The influence of osmotic stress to the surface structure of living cells was evaluated and also the contribution of exopolysaccharide and lipopolysaccharide (LPS) by imaging two mutant strains of the bacterium under native conditions. AFM images of living bacteria in culture medium exhibited surface structures of the size of single proteins emphasizing the usefulness of AFM for high resolution cell imaging.

© 2010 Elsevier B.V. All rights reserved.

1. Introduction

In order to gain structural information concerning the bacterial envelope, electron microscopy methods were mostly used. For example, scanning electron microscopy (SEM) can visualise topographic patterns of the bacterial surface, the freeze-fracture technique allows to image replicas of the membrane and its different layers [1] and transmission electron microscopy (TEM) images sections of the envelope [2]. Since samples for conventional SEM are examined in vacuum and often have to be fixed, dried and metal-coated [3], it is necessary to be aware of artefacts that might be introduced by sample preparation. Especially during the drying process, it is crucial to preserve natural structures [4], which can be altered by high surface tension occurring during water evaporation. To avoid these alterations, the medium is exchanged for organic solvents like isopropanol or acetone from which samples can be dried in air or by using critical point drying (CPD).

New developments in electron microscopy opened possibilities to image samples without some of the above mentioned preparative steps: for example, environmental scanning electron microscopy (ESEM) operates in low vacuum saturated with water so that samples might stay hydrated; using extreme high resolution scanning electron microscopy (XHR SEM) the electron beam can be decelerated shortly before reaching the sample to

approximately 50–2000 V. This allows imaging of the sample to a certain depth depending on the beam energy. A great advantage of these techniques is that no conductive coating is necessary anymore.

Atomic force microscopy (AFM) offers a similar lateral resolution compared to SEM and additionally gives very precise topological information over distances of several micrometers resulting in 3D topographic images [5]. Since this technique works in air as well as in liquid media AFM is well suited to analyse surface structures of biological material under native conditions [6] and living bacteria [7]. Thus, by using the latter microscopy method, different steps in sample preparation like fixation or drying can be omitted and the consequences regarding surface morphology can be compared.

We have chosen *S. meliloti* as model bacterium to investigate the surface morphology of gram-negative alpha-proteobacteria. The typical length scale of this rod-like bacterium ranges from 0.5 to 3 μm . *S. meliloti* is a symbiotic soil bacterium that is able to induce the formation of nodules on the roots of its leguminous host plants. These specialized plant organs are invaded by *S. meliloti* which can reduce and fix atmospheric nitrogen while being in an endosymbiotic organelle-like bacteroid state within the plant cell [8]. This process involves specific recognition of both bacterial and host cells. Symbiotic bacteria contribute significantly to an ecologically-sound and cost-efficient nitrogen supply. Additionally the non-pathogenic rhizobia are closely related to the important plant, animal and human pathogens such as *Brucella*, *Burkholderia* and *Ralstonia* allowing transfer of knowledge to these medically relevant bacteria [9]. *S. meliloti* is one of the best studied rhizobia. Its genome was sequenced [10] and a

* Corresponding author. Tel.: +49 521 106 5388; fax: +49 521 106 2959.

E-mail address: jan.regtmeier@physik.uni-bielefeld.de (J. Regtmeier).¹ Contributed equally.

number of post genomic approaches have been established for this organism. Therefore a lot of mutants have been established and are available for investigations.

The bacterial surface possesses unique structures that distinguishes it from the eukaryotic cell membrane but also enables a classification between different bacteria. Gram-negative bacteria feature a three-layered structure with inner and outer membranes which enclose the periplasm containing one layer of peptidoglycan [11]. The outer membrane is decorated with exopolysaccharides and lipopolysaccharides (LPS) being important endotoxins. LPS consists of lipid A that anchors the molecule to the membrane followed by core and O-antigen structures both based on carbohydrates [12]. This O-antigen is important, e.g. for the symbiotic interaction of some *Rhizobium*-strains and legumes [13,14]. Additionally some bacteria, but not *S. meliloti*, produce stiff capsules consisting of exopolysaccharides.

In this study we analyse the surface of *S. meliloti* by using different high resolution scanning microscopic techniques, namely SEM, XHR SEM and AFM in the dry and liquid phases. We compare surface patterns observed by these complementary methods under diverse environmental and preparative conditions. This experimental approach enables us to track the changes of native surface patterns introduced by every single step in preparation, starting from the most artificial conditions for SEM (fixed, dried, metal coated and high vacuum (HV)) to only softly immobilized living bacteria for AFM in the liquid phase. In order to clarify the origin of the surface patterns observed in the latter case, the impact of the osmolarity and two mutants of the wild type strain are studied. One strain lacks the ability to produce exopolysaccharides [15], the other has a defect in the LPS [16], the most dominant surface molecule of *S. meliloti*. Additionally we report on small protrusions present on the bacterial surface under native conditions that might represent single proteins of the outer membrane.

2. Materials and methods

2.1. Bacterial strains and culture conditions

The strains used in this study are listed in Table 1. *S. meliloti* strains, unless otherwise indicated, were grown at 28 °C in liquid cultures with Vincent minimal medium (VMM) [18] (1 mM MgSO₄, 250 μM CaCl₂, 10 mg/L FeCl₃, 1 mg/L biotin, 2 mM K₂HPO₄, 48.5 nM H₃BO₃, 10 nM MnSO₄, 1 nM ZnSO₄, 0.55 nM NaMoO₄, 0.27 nM CoCl₂, 10 g/L MOPS, 10 g/L mannitol, 3.55 g/L Na glutamate)

2.2. Chemicals and reagents

All chemicals and reagents were obtained from Sigma-Aldrich (Germany) including phosphate buffered saline (PBS) with 137 mM NaCl, 2.7 mM KCl and 10 mM phosphate, pH=7.4. All solutions were prepared with deionised water from a Milli-Q biocel (Millipore, USA). Poly(ethyleneimine) (PEI) 50% (w/v) in H₂O ($M_n \sim 60000$, $M_w \sim 750000$) was utilised. Paraformaldehyde was depolymerised in water at 60 °C and diluted in PBS before

glutaraldehyde was added to the solution. Parafilm (Pechiney Plastic Packaging) was purchased from VWR (Germany). Microscope and glass slides were purchased from Menzel (Germany).

2.3. SEM-imaging

For all experiments the glass was cleaned in an ultrasonic bath (Elma T 490DH), consecutively in acetone, ethanol and in MilliQ-H₂O for 20 s each and afterwards dried with nitrogen.

1 mL of the bacteria from the overnight cultures was washed twice with PBS buffer. Therefore the bacteria were centrifuged 5 min at 1500 rpm (Eppendorf centrifuge S417C), the supernatant was wasted and the pellet resuspended in 500 μL buffer. Washing was followed by fixation of the cells in 1.5% paraformaldehyde and 1.5% glutaraldehyde in PBS for 1 h at room temperature (RT). Afterwards the cells were washed again and resuspended in Milli-Q H₂O. For dehydration the water in the sample was slowly exchanged over at least 48 h against ethanol. Then after centrifugation (5 min at 1500 rpm) the ethanol was wasted and the pellet resuspended in 500 μL isopropanol. For drying 10 and 20 μL of each sample were dropped onto 8 by 8 mm² glass slides and dried in an isopropanol saturated atmosphere over at least 48 h at RT. For imaging the bacteria samples were sputtered with a 12 nm gold-layer (BAL TEC MED 020 coating system) and transferred into the scanning electron microscope (JEOL JSM-880).

2.4. XHR SEM imaging

For imaging with a XHR SEM (Magellan from FEI, Eindhoven, The Netherlands) the bacteria were treated as previously described for the SEM but without the slow drying procedure and metal coating.

2.5. AFM ambient imaging

AFM imaging in air was performed with a Multimode IIIa AFM (Veeco, USA) with a J-scanner operating in tapping mode. The silicon cantilevers Tap300Al (Budget Sensors, Bulgaria) with a nominal spring constant of 40 N/m were used. Samples were treated as described for SEM with the exception that no metal coating was applied.

2.6. AFM liquid phase imaging

For AFM imaging in liquid environment a MFP-3D (Asylum Research, USA) on an Olympus IX71 optical inverted microscope was used. Microbiolever AC40TS (Olympus, Japan), with a nominal spring constant of 0.1 N/m and a resonance frequency of 30 kHz in liquid, were used for tapping mode imaging. The scan rate was adjusted between 2 and 4.5 μm/s.

The microscope slides were functionalized with PEI as follows. First the glass slides were covered with Parafilm except the measurement region of about 6 cm². Then the Parafilm was firmly bond onto the glass at a temperature of ~50 °C for a few seconds on a hot plate. This results in a hydrophobic barrier preventing liquids to leave the measurement region during the coating process and the AFM imaging in the liquid phase. Then the inner region was coated using 1 mL of a 0.1% PEI solution in MilliQ-H₂O and incubated at RT for at least 30 min. The slide was thoroughly washed using MilliQ-H₂O and dried with nitrogen.

1 mL of the bacteria solution from the overnight cultures or after fixation with paraformaldehyde and glutaraldehyde as described for the SEM imaging was washed. Therefore the bacteria were centrifuged 5 min at 1500 rpm (Eppendorf centrifuge S417C), the supernatant was wasted and the pellet

Table 1
Strains used in this study.

<i>S. meliloti</i> strains	Description	Reference or source
Rm2011	Wild-type strain	[17]
Rm0540	exoY ⁻	[15]
Rm6963	LPS defect ⇒ short LPS	[14]

resuspended in either 500 μL PBS buffer, MilliQ-H₂O or VMM culture medium. The cells were pipetted onto the coated region of the microscope slide and incubated at RT for 1 h. Then the slide was thoroughly washed with MilliQ-H₂O and the fixed bacteria on the surface were kept hydrated for the AFM imaging using either 400 μL of PBS buffer, MilliQ-H₂O or VMM culture medium.

All obtained images (AFM und EM) have been processed and analysed using the image-acquisition software of Asylum-Research programmed using IgorPro 6.04 (WaveMetrics, USA) or SPIP-software (Image Metrology, Denmark).

3. Results

First we observed prominent wave-like surface patterns on metal coated *S. meliloti* (Rm2011) cells in SEM images (fixed, dried, metal coated and in vacuum) (see Fig. 1A). The protrusions possess a width of 29 ± 12 nm and are approximately 92 ± 31 nm long (mean \pm standard deviation (SD), number of measurements (N)=50). The gold-layer had a thickness of 12 nm. To exclude the possible surface alterations induced by metal coating, uncoated bacteria were systematically examined with XHR SEM (fixed, dried and in vacuum). In Fig. 1B elongated surface protrusions with a width of 18 ± 5 nm (mean \pm SD, N =50) and a length of 80 ± 27 nm (mean \pm SD, N =15) on the bacterial surface are clearly visible. Additionally, the high resolution of the XHR SEM images allowed detecting some round shaped protrusions of a diameter of 21 ± 4 nm (mean \pm SD, N =7). We may note that the interpretation of XHR SEM images should be exercised with caution as structures several nanometers below the surface might also be visible with the corresponding fainter contrast on the surface (see Section 4).

Quite similar results were achieved by imaging the bacteria with AFM under ambient conditions (bacteria fixed and dried). Here neither a metal coating nor vacuum is needed which could alter the appearance of the cells [19]. These images show the bacterial surface completely decorated with a dense network of surface protrusions of 12.1 ± 4.9 nm heights (mean \pm SD, N =47), 26 ± 6 nm lateral diameters (mean \pm SD, N =30) and 72 ± 28 nm lengths (mean \pm SD, N =65). The density of these wrinkled structures is so high that next to individual protrusions no flat

parts of the cellular membrane are visible (see Figs. 1C, 3A and 3B).

The diameters of the protrusions determined by XHR SEM and AFM are in good agreement bearing in mind the possible tip-convolution effects for AFM (see also Section 4). So the AFM results confirm that some of the structures hardly visible in XHR SEM images due to the faint contrast are actually present on the surface and not part of sub-surface structures.

In order to elucidate if the observed patterns are drying artefacts, AFM images were taken of glutaraldehyde- and paraformaldehyde-fixed *S. meliloti* bacteria (Rm2011) in PBS-buffer (see Figs. 2A and 4). There are protrusions present on the cells in liquid as well. Under these conditions they appear mostly round shaped with a height of 4.7 ± 2.7 nm (mean \pm SD, N =30) and a lateral diameter of 33 ± 8 nm (mean \pm SD, N =40).

Next, the fixation was omitted to evaluate potential surface alterations. Simultaneously, we changed the buffer to the fully defined Vincent minimal medium (VMM, 153 mosmol/L compared to 300 mosmol/L for PBS) to obtain more physiological conditions (see Fig. 2B). To underline that these changes do not hinder the comparability of the observed images, the influence of the osmolarity was cross-checked by imaging bacterial cells in pure water (see Fig. 2C). Under native conditions in VMM, the bacteria exhibit protrusions of a height of 4.0 ± 1.9 nm (mean \pm SD, N =46) and a width of 28 ± 6 nm (mean \pm SD, N =40) (see Figs. 2B and 5A left image). The dimensions are similar to chemically fixed bacteria in PBS-buffer. The higher osmolarity of the surrounding buffer-medium might have caused a slight shrinkage of the bacterial membrane since the protrusions are more pronounced in PBS than in culture medium or water. But even in water – a medium of lower osmolarity that might cause swelling of the membrane – similar protrusions are present (height 2.0 ± 0.7 nm, width 29 ± 10 nm (mean \pm SD, N =14), see Fig. 2C). In consequence, the observed structures are artefacts caused by neither fixation nor by environmental conditions but naturally occurring features on the bacterial envelope where just the height was slightly reduced depending on the low osmolarity of the used liquid phase.

To attribute the observed surface patterns to molecules present on the surface of the bacteria, two mutant strains were imaged without fixation by AFM in PBS buffer. The first strain (Rm0540) produces no exopolysaccharide (exoY⁻) (see Fig. 6) [15]. Here the

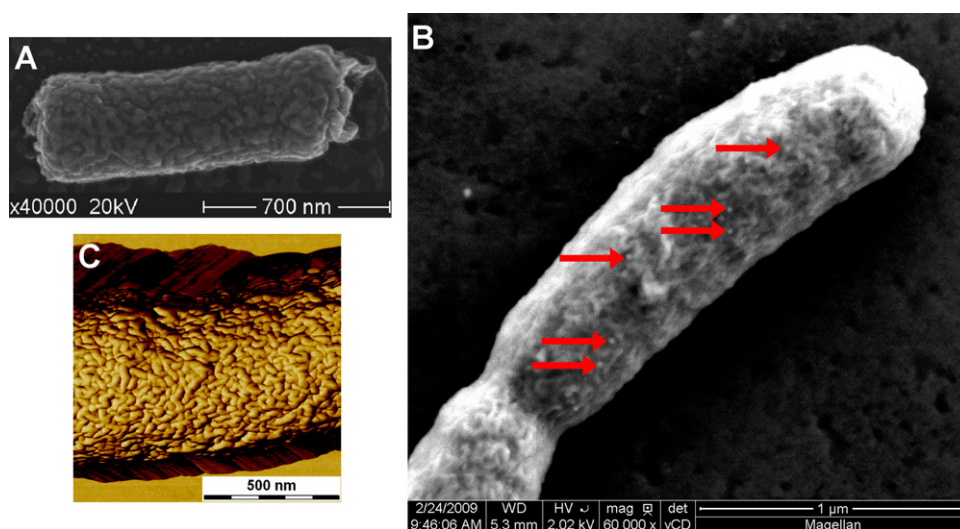


Fig. 1. Different microscopic techniques used to image the wild-type strain Rm2011: (A) SEM: fixed, dried, metal coated and imaged in vacuum. The bacterial surface is decorated with wrinkled protrusions. (B) XHR SEM: fixed, dried and imaged in vacuum. Different surface structures are discernible: elongated wrinkles cover most of the bacterium whereas several single dots are distributed over the surface (some examples marked by arrows). (C) AFM phase image: fixed, dried and imaged in air. The whole bacterial surface is covered with protrusions that show an elongated and wrinkled structure with no interspaces.

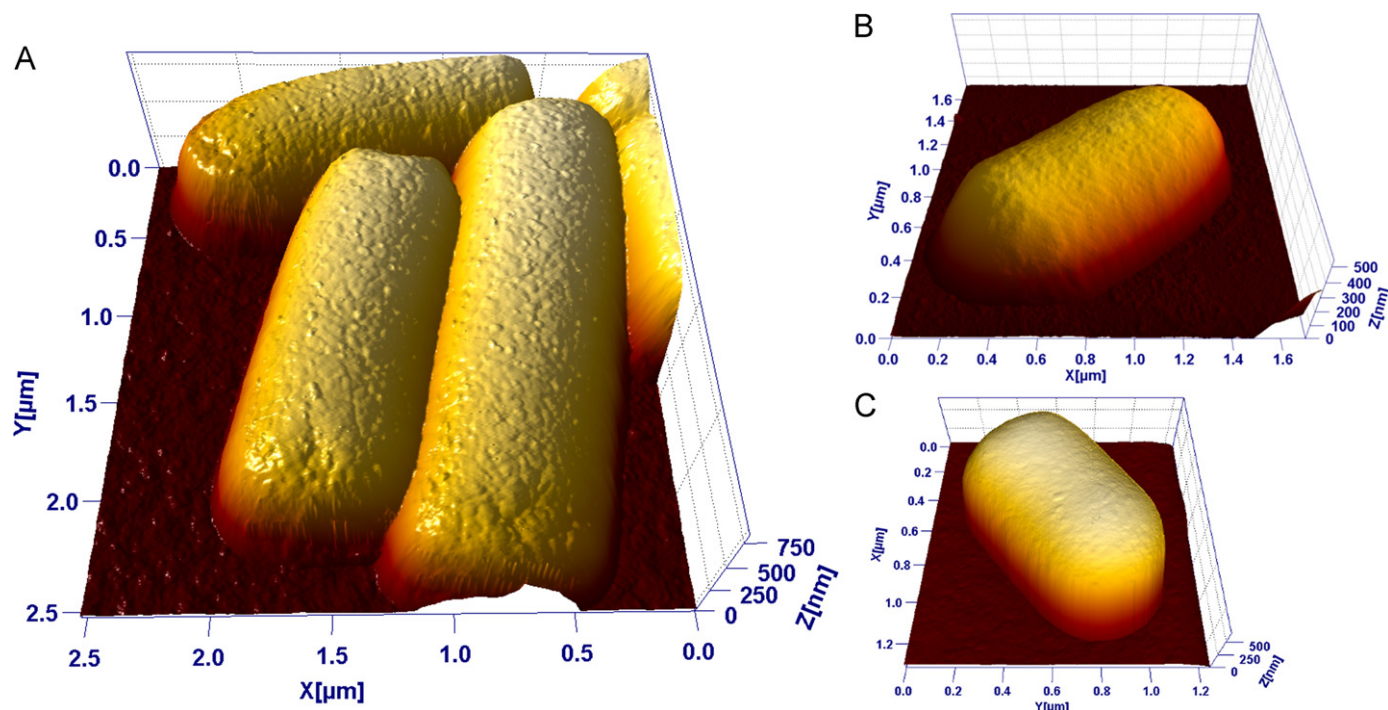


Fig. 2. AFM 3D height images of the topography of the wild-type strain Rm2011, under different conditions. (A) Fixed and imaged in PBS-buffer. The bacterial surface is completely decorated with round shaped protrusions. (B) Living bacterium in culture medium. Small protrusions can be recognized positioned closely together on the bacterial surface. (C) Living bacterium in water. Protrusions are present on the bacterial surface, but less pronounced than in PBS-buffer or VMM minimal medium of higher osmolarity.

surface of the living bacteria shows similar protrusions but the height of these structures is almost doubled (9.0 ± 6.5 nm (mean \pm SD, $N=54$), diameter 45 ± 8 nm, (mean \pm SD, $N=20$)) compared to the wild-type strain in PBS buffer (see Figs. 2A and 4 left image). In good approximation the height of the protrusions reaches the value obtained for fixed and dried bacteria of the wild-type strain (Rm2011).

The effect of the LPS-layer on the surface of the bacteria was investigated by imaging mutant strain Rm6963. This strain only produces a truncated form of LPS consisting of the lipid A and a smaller core region followed by the intact O-antigen [16]. The AFM images of the living bacteria in culture medium yielded a height of the surface patterns of 1.6 ± 0.6 nm (mean \pm SD, $N=19$) (see Fig. 5B right image), with clearly less pronounced protrusions compared to the wild-type bacteria (see Section 4).

4. Discussion

Three different aspects should be discussed in more detail: firstly, methodical requirements concerning AFM sample preparation and imaging; secondly, interpretations and consequences for sample preparation; and thirdly, possible explanations concerning the origin of the observed protrusions under most native conditions (AFM in liquid with living bacteria).

4.1. Methodical requirements

Earlier, silicon nitride AFM cantilevers were used in liquids because of the low spring constant. However, the aspect ratio and tip radius are not as good as for silicon tips typically used under ambient conditions. To yield a better comparability and higher resolution, hybrid cantilevers were used in liquids consisting of a silicon nitride lever with a silicon tip that possesses a similar geometry to the tips used in air. Therefore, the steep sidewalls of

the bacteria cause less imaging artefacts [20] and the resolution is improved.

Additionally, it is noteworthy that functionalizing the glass slides with PEI is as simple but less expensive than using polylysine, retaining the electrostatically induced tight immobilization. This enables stable images of good resolution, which is sometimes difficult to achieve in aqueous media. Moreover, our own long-time observations for the collection of time lapse fluorescence imaging (TLFI) data of different *S. meliloti* strains fixed with PEI in a microfluidic chip revealed a high viability of the cells, supported by doubling-times close to the doubling-time in liquid [21].

4.2. Surface modification due to sample preparation

Comparing AFM images of bacteria in liquid with and without fixation, no obvious change in surface morphology could be observed (Fig. 2A and B). On dried bacteria, more wave-like patterns are present instead of round protrusions (see AFM in air (Figs. 1C, 3A and 3B), XHR SEM (Fig. 1B) and SEM (Fig. 1A)). One could think of several mechanisms responsible for wrinkle formation. One possibility is the wrinkling of the approximately 20 nm thick bacterial envelope (19–24 nm have been determined for *Escherichia coli* earlier [22]). The wrinkles observed with XHR SEM have a width of 18.4 ± 4.3 nm. Therefore, a wrinkling of the entire envelope can be excluded due to the dimensions. But as observed before, it is possible that membrane layers separate during drying [1] or form a plasmolysis space in response to osmotic stress [22], and a wrinkling of only the outer layer would yield in the right dimensions. A second possibility is the formation of elongated wrinkles by the coalescence of round protrusions. During the drying process the stress on the linking between the layers of the membrane will increase so that the round protrusions seen in liquid can fuse to form elongated wrinkles. This is supported by the similitude of the diameters of the round

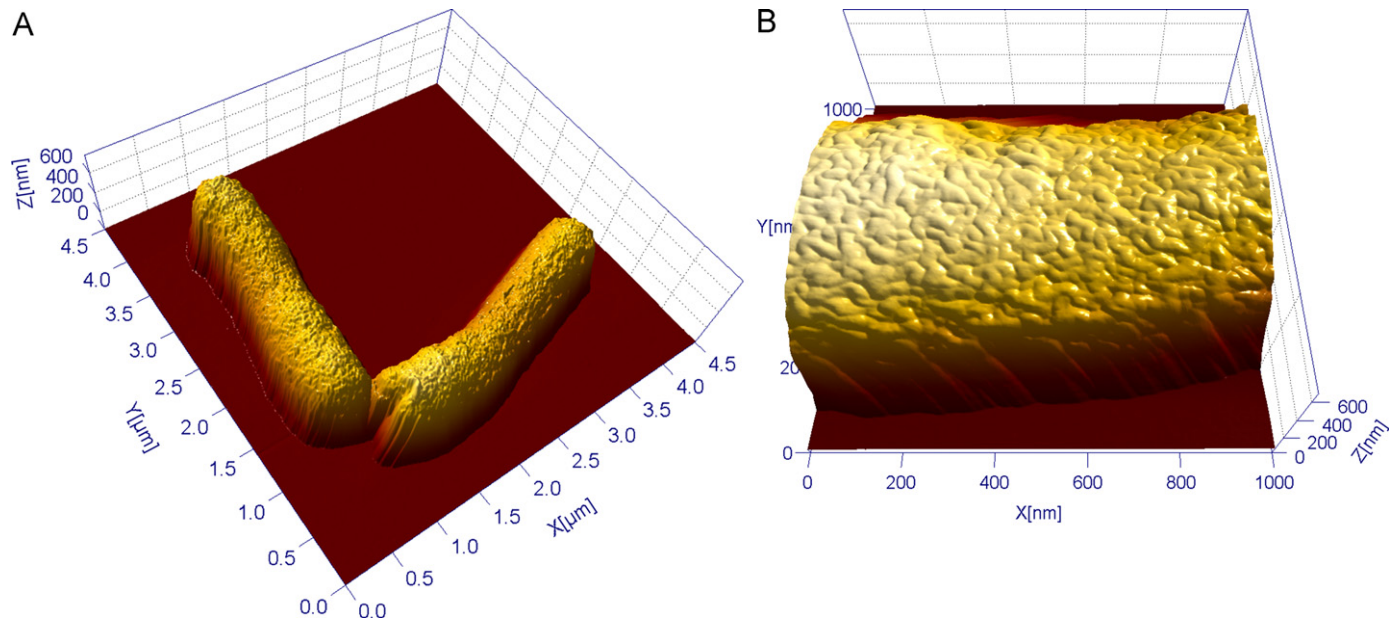


Fig. 3. AFM images of the wild-type-strain Rm2011, fixed, dried and imaged in air. The whole bacterial surface is covered with protrusions (A, 3D height data) that show a elongated and wrinkled structure with no interspaces (B, 3D height data of a magnified part)

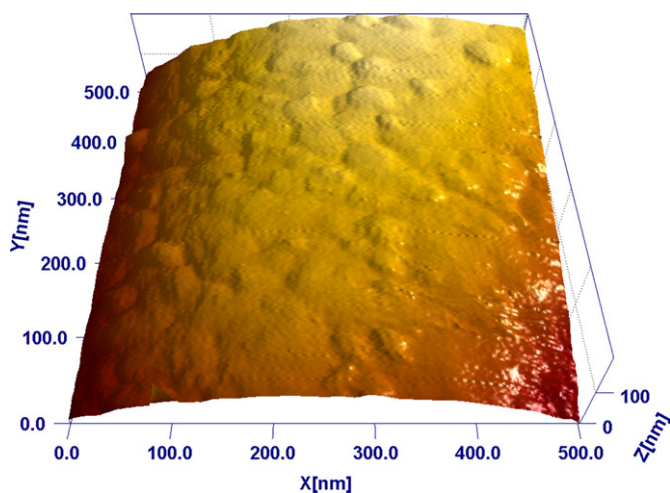


Fig. 4. AFM 3D images of the topography of the wild-type strain Rm2011, fixed and imaged in PBS-buffer. The bacterial surface is completely decorated with round shaped protrusions (high resolution scan).

protrusions (28 ± 6 nm (mean \pm SD, $N=40$), Figs. 2B and 5A) in comparison to the width of the elongated patterns (26 ± 6 nm (mean \pm SD, $N=30$), Figs. 1C, 3A and 3B).

Comparing SEM and XHR SEM images (see Fig. 1A and 1B) smaller structures can be resolved in XHR SEM images. While the width of the protrusions is approximately 11 nm smaller in XHR SEM images, the additional gold layer used for SEM could explain the observed difference. Smaller protrusions might be covered by the metal-layer in the SEM images and could appear as broader protrusion e.g. when two structures are positioned close to each other. Using thinner metal layers for SEM imaging (e.g. tantalum or iridium), these should become observable.

4.3. Origin of round protrusions

AFM imaging of living cells in buffer comes closest to physiological conditions. Therefore, we argue that the observed

surface patterns on living cells with AFM in liquids are naturally occurring and would like to discuss different possible origins of these.

One explanation could be a pushing of proteins or complexes thereof against the membrane from the inside. It is known that between the inner and outer membrane of gram-negative bacteria, a large number of proteins are located (diameter 6–10 nm) [1]. So it is possible that some of these are pressed against the flexible outer membrane. This could also explain the increased height of the patterns on dried bacteria as the membrane might partially enclose some of these particles during the drying process.

Another cellular process responsible for protrusions could be the formation of membrane vesicles budding of the outer membrane as described before and pre-stages thereof [23,24]. The formation of vesicles by *S. meliloti* is an active field of research especially concerning the dependence of formation on molecular cues. As the fully extended vesicles have typical diameters of 50–250 nm, the protrusions described here might be precursors of these vesicles. Whether no large vesicles are formed, e.g. because of lacking stimulation or if they are sheared off by the AFM tip, should be studied in the future.

It was proposed that vesicle might form in areas where the linkage of the outer membrane and the peptidoglycan is weakened, e.g. because of remodelling processes [24]. If the linkage was distorted in small areas only it might be possible for the outer membrane to generate protrusions without generating vesicles. Concerning the elongated protrusions observed on dried bacteria, increasing the stress on the remaining linking structures because of drying could lead to linkage distortion and fusion of the round protrusions (AFM in air, Figs. 1C, 3A and 3B; XHR SEM, Fig. 1B and SEM, Fig. 1A). Please note, as the lipids forming the vesicles are not chemically fixed (e.g. with OsO_4), the fully extended vesicles are not expected to be observable in (XHR) SEM and AFM images recorded in air.

The mechanisms discussed so far are also supported by the dependence of the surface patterns on osmolarity. Slight swelling or shrinking would pronounce or diminish such effects below the outer membrane, as observed in the corresponding AFM images (Fig. 2A–C).

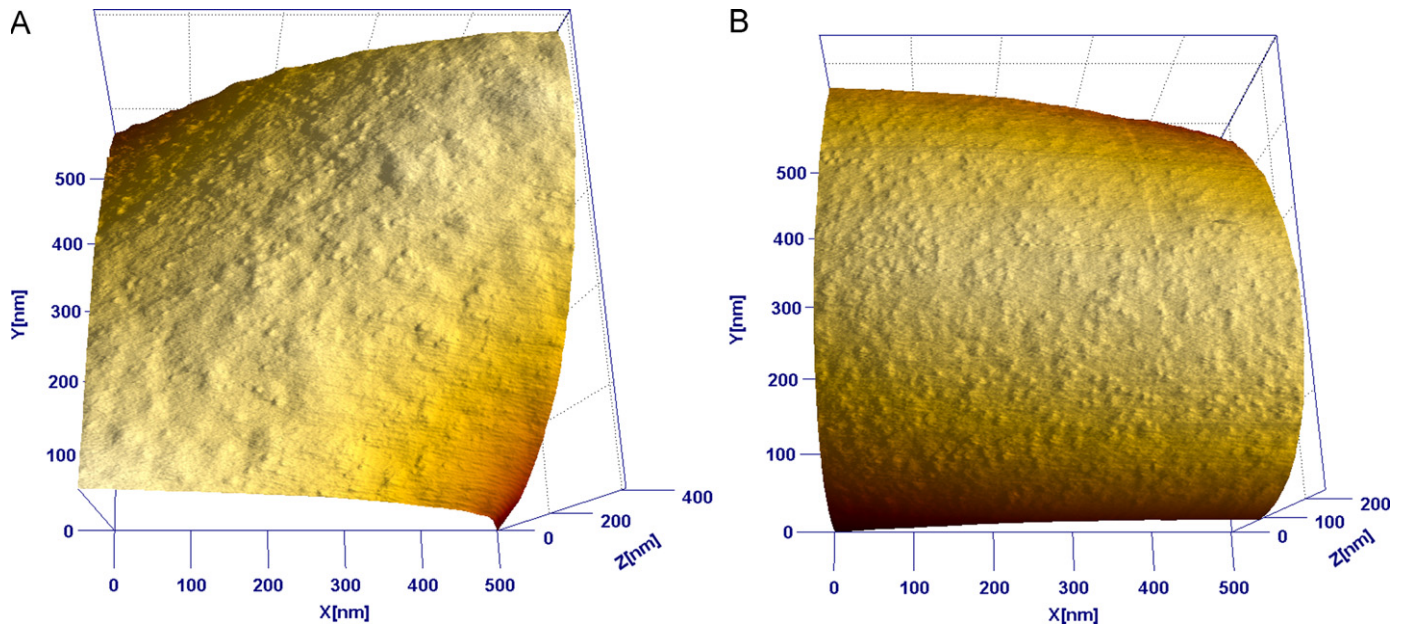


Fig. 5. High-resolution AFM scans of wild-type (A, 3D height data) and LPS-deficient strain (B, 3D height data) living bacteria imaged in culture medium. Small protrusions on the surface might represent the extracellular part of single proteins (e.g. outer membrane proteins, Omp).

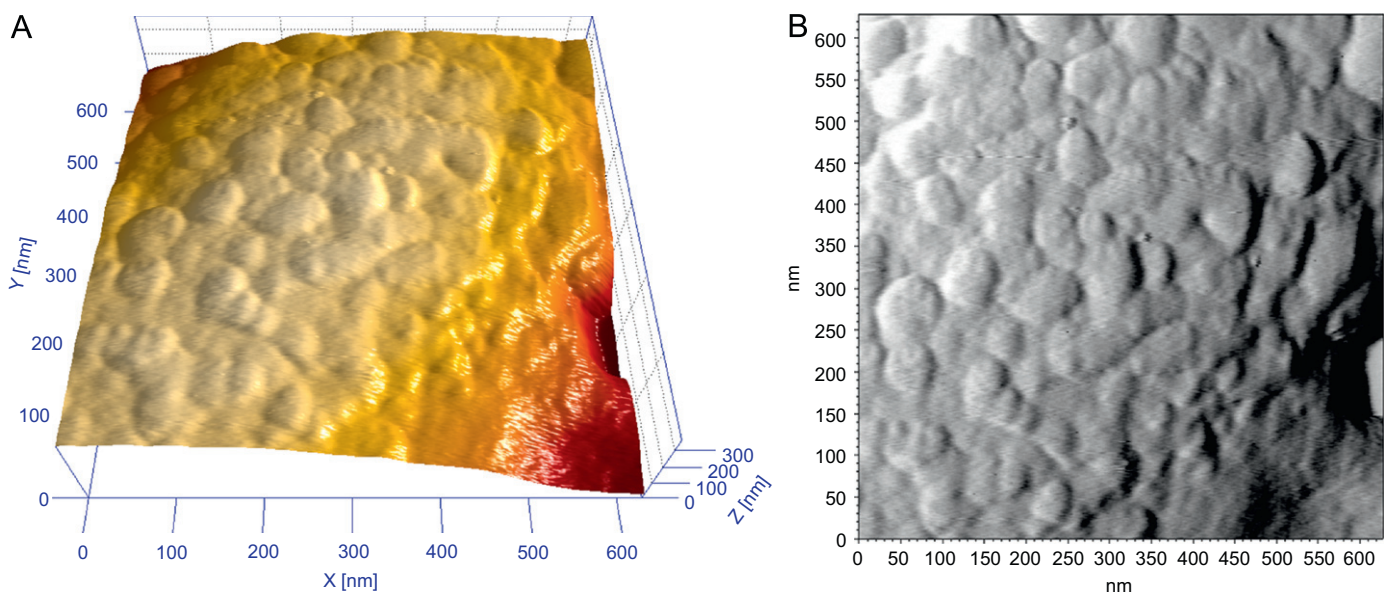


Fig. 6. AFM 3D height image (A) and amplitude image (B) of a high resolution scan of the *exoY*⁻ mutant strain Rm0540 living bacterium in PBS. The protrusions on the surface are more pronounced than in other strains indicating that normally exopolysaccharides cover these membrane structures.

The impact of exopolysaccharides and the LPS layer on surface patterns was specifically addressed with two mutant strains. For the mutant lacking the exopolysaccharides, similar surface patterns compared to the wild-type strain are observed but the height of the structures is almost doubled. Thus, the exopolysaccharides cannot be the origin of the patterns. But the drying seems to have a similar effect on the height of the surface patterns compared to the absence of the exopolysaccharides. This seems plausible because this layer might be more compact when imaged in air because of a loss of bound water and partial extraction of the molecules during preparation.

The protrusions of the mutant with a truncated form of LPS (height 1.6 ± 0.6 nm (mean \pm SD, $N=19$)) are less pronounced than for the wild type (height 4.0 ± 1.9 nm, $N=46$). So for both strains they are significantly lower than the length of complete

LPS molecules (6–45 nm) [25,23]. The AFM tip in the liquid phase can easily push aside the highly flexible structures and it is therefore assumed that only the lipid A and core oligosaccharides are detected using AFM-imaging [23]. The height of the protrusions of the wild type is in accordance with the reported thickness of this part of an intact LPS-layer (extracted from *Pseudomonas aeruginosa* 5–6 nm [23], on the surface of *E. coli* 4 nm [25]). Since Rm6963 synthesizes an LPS with a truncated core oligosaccharide [16] the reduction of height of the protrusions by 2 nm compared to the wild type supports the assumption that these structures represent LPS-patches covering major parts of the cell surface as described earlier for *E. coli* [25].

Besides the already discussed protrusions, two additional sorts of patterns were observed. First, there are small dots present on the bacterial surface imaged with AFM in culture medium

(Rm2011 height 2.0 ± 0.6 nm, diameter 12 ± 3 nm (mean \pm SD, $N=20$), see Fig. 5A; Rm6963 height 1.3 ± 0.5 nm, diameter 14 ± 4 nm (mean \pm SD, $N=40$), see Fig. 5B). With respect to the small size and taking into account the tip-convolution, these might be proteins that are associated with the outer membrane. Many outer membrane proteins (Omp) of gram-negative bacteria are based on a beta-barrel structure with a diameter of 14–40 Å [26]. The extracellular part of OmpF from *E. coli* surmounts the membrane by 1.1 ± 0.2 nm [27], which is in good agreement with the reported height.

Secondly, in XHR SEM round protrusions of 21 ± 4 nm (mean \pm SD, $N=7$) diameter are visible (see Fig. 1B marked with arrows). As noted before, XHR SEM allows to look beneath the surface and therefore it is difficult to decide whether the objects are on the surface or just beneath. If the observed patterns are beneath, they could be interpreted as ribosomes, which have a diameter of approximately 20 nm and are expected just beneath the bacterial envelope [28,29].

5. Conclusion

In this study we characterized the gram-negative bacterium *S. meliloti* with respect to surface patterns typically found in SEM data by different SEM and AFM techniques. With those complementary methods every preparative step could be evaluated concerning the generation of image artefacts. With AFM in liquids, natively occurring round surface protrusions were observed with height depending on osmolarity. Possible causes were discussed including contributions of LPS and exopolysaccharides. It could be demonstrated that drying led to the generation of elongated wrinkles and argued that these may evolve from the former round protrusions.

The observation of 2 nm high protrusions, interpreted as proteins on the surface of living bacteria, stresses the obtainable resolution and the eligibility of liquid AFM for high resolution biological studies.

Acknowledgement

We want to thank Prof. Karsten Niehaus from the Department of Proteome- and Metabolome-Research for fruitful discussions, Christoph Pelargus for SEM support and Andreas Hütten for the

image shown in Fig. 2 taken during a demo session at the FEI laboratory, Eindhoven, The Netherlands. D.A. acknowledges support from BASF, Germany, within a joint research project on biofilm formation.

References

- [1] M.E. Bayer, C.C. Remsen, *J. Bacteriol.* 101 (1970) 304–313.
- [2] J. Dubochet, A.W. McDowell, B. Menge, E.N. Schmid, K.G. Lickfeld, *J. Bacteriol.* 155 (1983) 381–390.
- [3] L.P. Watson, A.E. McKee, B.R. Merrell, *Scan. Electron. Microsc.* (1980) 45–56.
- [4] L. Bergmans, P. Moisiadis, B. Van Meerbeek, M. Quiryne, P. Lambrechts, *Int. Endod. J.* 38 (2005) 775–788.
- [5] D. Anselmetti, N. Hansmeier, J. Kalinowski, J. Martini, T. Merkle, R. Palmisano, R. Ros, K. Schmied, A. Sischka, K. Toensing, *Anal. Bioanal. Chem.* 387 (2007) 83–89.
- [6] D.J. Muller, A. Engel, *Nat. Protoc.* 2 (2007) 2191–2197.
- [7] V. Dupres, D. Alsteens, K. Pauwels, Y.F. Dufrene, *Langmuir* (2009) 9653–9655.
- [8] K.M. Jones, H. Kobayashi, B.W. Davies, M.E. Taga, G.C. Walker, *Nat. Rev. Microbiol.* 5 (2007) 619–633.
- [9] P. Mergaert, T. Uchiumi, B. Alunni, G. Evanno, A. Cheron, O. Catrice, A.E. Mausset, F. Barloy-Hubler, F. Galibert, A. Kondorosi, E. Kondorosi, *Proc. Natl. Acad. Sci. U.S.A.* 103 (2006) 5230–5235.
- [10] F. Galibert, et al., *Science* 293 (2001) 668–672.
- [11] J.W. Costerton, J.M. Ingram, K.J. Cheng, *Bacteriol. Rev.* 38 (1974) 87–110.
- [12] C.R. Raetz, *Annu. Rev. Biochem.* 59 (1990) 129–170.
- [13] J.R. Cava, P.M. Elias, D.A. Turowski, K.D. Noel, *J. Bacteriol.* 171 (1989) 8–15.
- [14] A. Lagares, G. Caetano-Anolles, K. Niehaus, J. Lorenzen, H.D. Ljunggren, A. Puhler, G. Favelukes, *J. Bacteriol.* 174 (1992) 5941–5952.
- [15] K. Niehaus, D. Kapp, A. Puhler, *Planta* 190 (1993) 415–425.
- [16] K. Niehaus, A. Lagares, A. Puhler, *Mol. Plant-Microbe Interact.* 11 (1998) 906–914.
- [17] F. Casse, C. Boucher, J.S. Julliot, M. Michel, J. Denarie, *J. Gen. Microbiol.* 113 (1979) 229–242.
- [18] J.M. Vincent, in: *A Manual for the Practical Study of the Root-Nodule Bacteria*, Blackwell Scientific publishers, Oxford-Edinburgh, 1970.
- [19] S.H. Coetzee, A. Jordaan, S.F. Mpuchane, *Microsc. Res. Tech.* 67 (2005) 265–270.
- [20] S.B. Velegol, S. Pardi, X. Li, D. Velegol, B.E. Logan, *Langmuir* 19 (2003) 851–857.
- [21] D. Greif, N. Pobigaylo, A. Becker, J. Regtmeier, D. Anselmetti, *Proc. μ TAS 2009* (2009) 412–414.
- [22] H. Schwarz, A.L. Koch, *Microbiology* 141 (1995) 3161–3170.
- [23] T.J. Beveridge, *J. Bacteriol.* 181 (1999) 4725–4733.
- [24] B.L. Deatherage, J.C. Lara, T. Bergsbaken, S.L. Rassouljian Barrett, S. Lara, B.T. Cookson, *Mol. Microbiol.* 72 (2009) 1395–1407.
- [25] N.A. Amro, L.P. Kotra, K. Wadu-Mesthrige, A. Bulychev, S. Mobashery, Gy Liu, *Langmuir* 16 (2000) 2789–2796.
- [26] G.E. Schulz, *Biochim. Biophys. Acta* 1565 (2002) 308–317.
- [27] F.A. Schabert, C. Henn, A. Engel, *Science* 268 (1995) 92–94.
- [28] L.L. Randall, S.J. Hardy, *Eur. J. Biochem.* 75 (1977) 43–53.
- [29] A.A. Herskovits, E. Bibi, *Proc. Natl. Acad. Sci. U.S.A.* 97 (2000) 4621–4626.